Measurement of the Length and Strength of Adhesive Interactions in a Nanoscale Silicon–Diamond Interface

Tevis D. B. Jacobs, Joel A. Lefever, and Robert W. Carpick**

The adhesive interactions between nanoscale silicon atomic force microscope (AFM) probes and a diamond substrate are characterized using in situ adhesion tests inside of a transmission electron microscope (TEM). In particular, measurements are presented both for the strength of the adhesion acting between the two materials (characterized by the intrinsic work of adhesion $W_{adh,int}$) and for the length scale of the interaction (described by the range of adhesion z_0). These values are calculated using a novel analysis technique that requires measurement of the AFM probe geometry, the adhesive force, and the position where the snap-in instability occurs. Values of W_{adh} = 0.66 J m^{-2} and z_0 = 0.25 nm are extracted using this technique. This value of work of adhesion is 70% higher than the work of adhesion calculated if one uses a conventional paraboloidal asperity model. Comparing to literature, the work of adhesion obtained using the new method is significantly higher than most experimental and simulation values for similar material pairs. The discrepancy is attributed to nanoscale roughness, which was not accounted for previously. Furthermore, the value of the range of adhesion is comparable to previously reported values, but is significantly larger than the commonly assumed value of the interatomic spacing.

1. Introduction

Accurate characterization of adhesion is critical for the design and commercial use of nanoscale devices.[1] It is also needed to understand the relationship between surface chemistry and adhesion, i.e., without the complicating effects of roughness. Fortunately, well-established adhesion models[2,3] exist to predict adhesive forces for arbitrary geometries. However, even for effectively rigid bodies, these models require knowledge of the intrinsic parameters governing the adhesive interaction in addition to the geometry of the bodies. In the common, two-variable descriptions of adhesion,[4–8] these parameters are the strength of the adhesive interaction (characterized by the intrinsic work of adhesion $W_{adh,int,}$) and the length scale of the interaction (characterized by the range of adhesion z_0).

The intrinsic work of adhesion W_{adh} is the energy per unit area required to separate two planar surfaces from equilibrium contact to infinite separation. In terms of surface energy (γ_i of surface i) and interfacial energy (γ_{ij} between surfaces i and j), the work of adhesion is calculated as follows:

$$W_{adh} = \left(\gamma_i + \gamma_j\right) - \gamma_{ij} \tag{1}$$

In accordance with prior literature on adhesion and roughness,[9] the intrinsic work of adhesion $W_{adh,int}$ is defined as the work of adhesion between two perfectly flat, planar surfaces. While $W_{adh,int}$ is a continuum concept, it can be robustly mapped onto an atomistic description of two atomically flat, single-crystal surfaces in contact. The effective work of adhesion, $W_{adh,eff}$, is defined as the work of adhesion for the same material pair and the same global geometry (planar), but with the addition of local surface roughness on one or both surfaces. The distinction between $W_{adh,int}$ and $W_{adh,eff}$ is shown schematically in **Figure 1**. The $W_{adh,int}$ is determined by the identity of the materials in contact, and the environment, whereas $W_{adh,eff}$ is a function of $W_{adh,int}$ and the local surface topography. For hard, non-conforming materials, $W_{adh,eff}$ is typically much smaller than $W_{adh,int}$. The primary reason for this is that the roughness increases the effective separation between the two materials, and therefore significantly increases γ_{ij} between the materials as they can no longer make intimate contact. Roughness can also increase the surface energies γ_i and γ_j, but this effect is typically overwhelmed by the change in γ_{ij}. This distinction is drawn because many experimental techniques exist to measure $W_{adh,eff}$ (for example, using microfabricated beam tests[10]), but generally applicable techniques to deduce from this the $W_{adh,int}$ are not well established.

Physically, z_0 describes the equilibrium separation distance between perfectly flat surfaces, i.e., the separation distance at which their interaction force is zero. However, in many mathematical descriptions of adhesion (for instance, refs. [5,7,8,11]) z_0 also scales the distance over which adhesion acts for a particular material. Therefore, the parameter z_0 is referred to in this paper as the "range of adhesion," (in accordance with Greenwood,[5] who calls it the "range of action of the surface forces").

Prof. T. D. B. Jacobs
538-E Benedum Hall
3700 O'Hara St, Pittsburgh, PA 15208, USA
E-mail: tjacobs@pitt.edu
J. A. Lefever
3231 Walnut St., Philadelphia, PA 19104, USA
Prof. R. W. Carpick
229 Towne Bldg
220 S. 33rd St., Philadelphia, PA 19104, USA
E-mail: carpick@seas.upenn.edu

DOI: 10.1002/admi.201400547

© 2015 WILEY-VCH Verlag GmbH & Co. KGaA, Weinheim

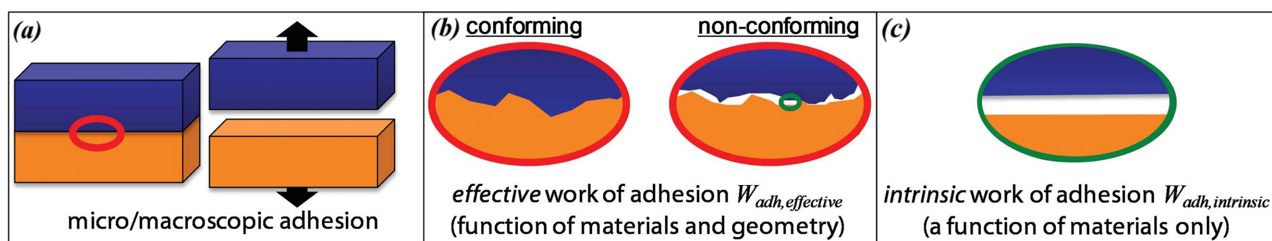

Figure 1. Intrinsic and effective works of adhesion can differ significantly. a,b) A micro/macroscopic adhesion test typically measures an effective value, due to roughness of the contact. c) The intrinsic work of adhesion describes contact between perfectly flat surfaces and is therefore determined solely by the materials in contact.

In previous reports (for example [12]) simplifying assumptions—such as simple geometries, or an estimated value of z_0—are required in order to analyze adhesion using continuum models. In other cases, geometry-dependent tip/sample interaction parameters can be determined. For example, one can use conventional AFM where snap-in can be avoided (i.e. for sufficiently weak adhesion and/or sufficiently stiff cantilevers, thus requiring extremely high sensitivity[13]). Alternately, dynamic AFM modes[14–16] or force-feedback instrumentation can be used.[16–19] However even with such techniques, without knowledge of the tip geometry, only effective parameters can be determined. We have developed a technique, the Snap-in/pull-off Numerical Adhesion Parameter (SNAP) method, in which AFM-like adhesion tests are performed using tips of precharacterized geometry. This allows simultaneous extraction of both $W_{adh,int}$ and z_0; the technique is summarized in the methods section—technical details can be found elsewhere.[20]

In the present paper, this technique is applied to silicon AFM probes (with native oxide) in contact with a flat single-crystal diamond punch in order to measure $W_{adh,int}$ and z_0 for this interface. Silicon is widely used for microscopy and device applications. Ultra-hard, diamond-like materials are emerging as solutions to reduce friction, adhesion, and wear of the same components.[21] Therefore, interfaces between these two materials have significant technological relevance.

We first review many of the important prior investigations into nano- and microscale adhesion, which report values for the work of adhesion W_{adh} of two contacting surfaces. We organize these prior investigations into two broad categories: measurements performed on nominally planar interfaces using microfabricated devices/surfaces; and measurements performed using nonplanar, single-asperity contacts.

Several significant adhesion investigations have been performed, primarily on silicon, using techniques and materials from the semiconductor and microfabrication industry, such as microfabricated cantilever beams[10,22] and direct wafer bonding.[23] These studies used micro- and macroscale devices to perform experiments, and analyzed results using well-established elasticity and fracture mechanics theories. In these analyses, the contacting surfaces were treated as flat, and measurements were made of the energy per unit of nominal contact area required to separate them. For self-mated silicon interfaces, these studies report effective work of adhesion values in the range of $W_{adh,eff} = 0.010–0.250$ J m^{-2}, [24,25] and demonstrate the significant effect of surface chemistry, surface roughness, and ambient environment.

As mentioned, the present article follows the convention of Persson[26] and designates values measured on rough surfaces as effective works of adhesion $W_{adh,eff}$, distinct from the intrinsic work of adhesion $W_{adh,int}$, which is the value used in continuum models, which would be measured on perfectly flat surfaces composed of the same material pair. This distinction is illustrated by delRio et al.[22] The authors performed a micrometer-scale cantilever beam experiment, with additional characterization of the nanoscale surface topography of both contacting surfaces using atomic force microscopy. The contacting materials (silicon beams coated with a low-adhesion fluorocarbon monolayer in contact with a silicon substrate with a native oxide) were estimated to have an intrinsic work of adhesion of approximately 33 mJ m^{-2}, but an effective work of adhesion for the whole cantilever beam of less than 0.010 mJ m^{-2}. This large difference arises because of the roughness of the interfaces, which reduces the average separation of the two bodies, and thus significantly reduces the interfacial energy γ_{12} of their contact. This illustrates a limitation of the above measurements of $W_{adh,eff}$, as they depend sensitively on the exact geometry and final roughness of the surfaces in contact. Therefore, results cannot be easily generalized from one contacting interface to another.

A second category of adhesion investigations uses nanoscale, single asperity contacts, and attempts to extract the intrinsic work of adhesion $W_{adh,int}$. This quantity is the correct one for use in continuum contact models[4–6,8,27,28] as well as in roughness models.[26,29,30] The investigations in this second category have employed the atomic force microscope (AFM),[8,12,31–34] the related interfacial force microscope (IFM),[35] and the surface forces apparatus (SFA)[36,37] to conduct adhesion tests with high-force resolution using a single-asperity contact, typically on the nanometer length scale. Since these are not flat surfaces, a value for work of adhesion requires using a contact mechanics model to fit the data. By applying certain assumptions, the work of adhesion can be extracted. For example, Grierson[31] describes a general method for extracting work of adhesion from AFM pull-off force data, and the authors go on to measure work of adhesion values for silicon tips on silicon substrates. Other researchers[12,32,33] applied similar techniques with silicon- and/or carbon-based interfaces. Burnham[34] carried out extensive pull-off force measurements between silicon AFM tips and silicon substrates and analyzed results using a related approach. In another study, the IFM was used to study a silicon/silicon interface under a variety of conditions.[35] Results varied widely between different tests, even for similar

© 2015 WILEY-VCH Verlag GmbH & Co. KGaA, Weinheim

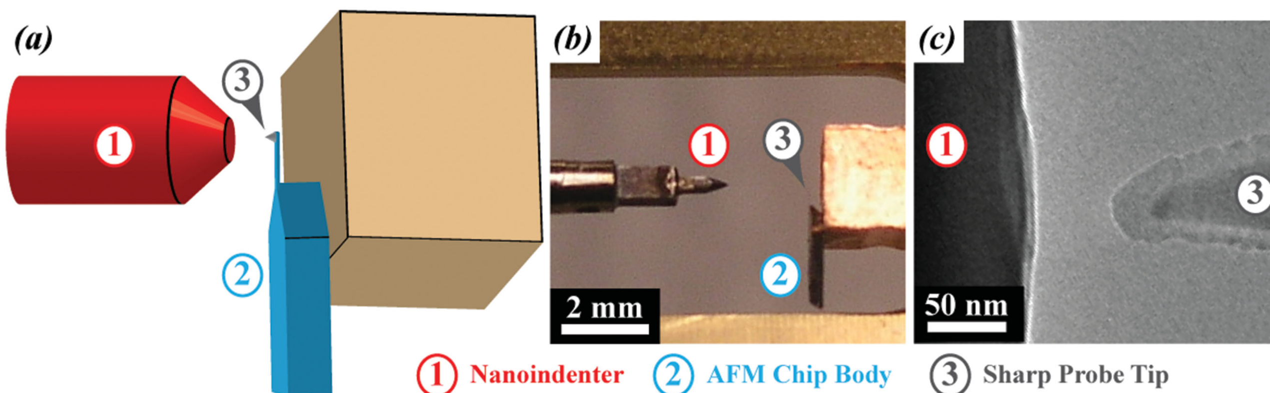

Figure 2. An in situ indentation apparatus is used for adhesion tests. The AFM probe is mounted on the sample surface such that its tip is accessible by the nanoindenter punch, as shown a) schematically and b) in an optical photograph. c) Once inside the TEM the flat punch indenter (left, dark) is brought into adhesive contact with the nanoscale AFM probe tip (right, lighter gray). Reproduced with permission.[42] Copyright 2013, Springer.

conditions. For instance, for self-mated silicon interfaces (with a native oxide) in air, work of adhesion values were reported to range from[32] 0.040 J m^{-2} up to[12] 0.83 J m^{-2}—likely due to differences in roughness and surface preparation. Quantitative results from each of the above studies, and from related molecular dynamics simulations, are presented in the Discussion section. A limitation of all of the above measurements is that the sharp tip is assumed to be a paraboloid, as required by typical contact mechanics models (DMT, JKR, Maugis),[4,27,28] but the detailed geometry and roughness of the nanoscale tip are unknown.

More recently, adhesion tests have been performed using tips that have been precharacterized using transmission electron microscope (TEM).[8,38–42] Such investigations enable more accurate application of contact mechanics models, especially characterizing the probe apexes and then modeling them as paraboloidal[40,41] or higher-order power-law[8] geometries, or as shapes with nanometer- and Ångström-scale roughness.[42] These investigations alleviated the need for some of the geometric assumptions of previous studies, and demonstrated how probe shapes can change with sliding[8,40,41] and the strong effect of roughness on apparent measurements of work of adhesion $W_{adh,eff}$.[42] However, a significant remaining limitation of these investigations is the need to assume a certain value for the range of adhesion z_0.

While many detailed investigations of adhesion have been carried out, values for the range of adhesive interactions have not been well characterized. Several studies have estimated a value using order-of-magnitude arguments, then used this estimated value to accurately fit experimental data.[7,43–47] Values have ranged from 0.1 up to 4–5 nm for a variety of materials, as described in more detail in the Discussion section. However, none of these techniques enable a robust method for extracting reliable values for both z_0 and $W_{adh,int}$. The present technique (the SNAP method, described in the methods section) is used to accomplish this.

2. Results of In Situ Adhesion Testing, and Extracting Adhesion Parameters

Adhesion tests using AFM tips were performed in the TEM. Then, a common two-parameter adhesion description was integrated over the true shape of the AFM probe. Fitting the computed pull-off force and snap-in distance to the actual values, enabled simultaneous extraction of the work of adhesion and the range of adhesion. In the present investigation, a modified in situ TEM nanoindenter, shown in **Figure 2**, was used to conduct the tip characterization and adhesion testing in the same apparatus, as described in the Methods section.

The three tested tips are shown in **Figure 3** and an example video of an adhesion test is presented in the Supporting Information. Extracted still frames from the adhesion video are shown **Figure 4**, and demonstrate the measurement of the

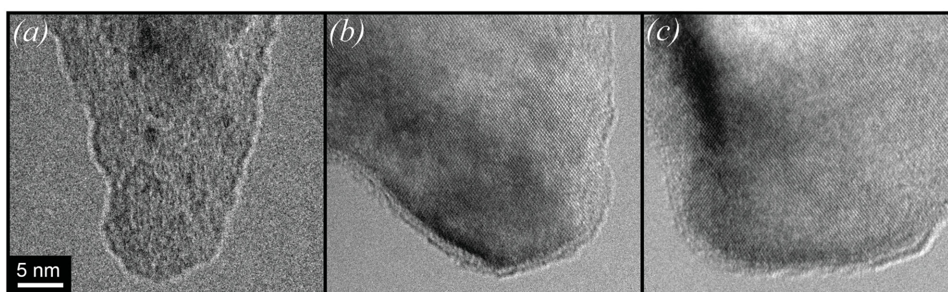

Figure 3. In situ adhesion tests were performed on three silicon AFM probes with a native oxide. The three tips are shown here at a common magnification. The overall shape and local roughness of the probes vary across the three tips.

© 2015 WILEY-VCH Verlag GmbH & Co. KGaA, Weinheim

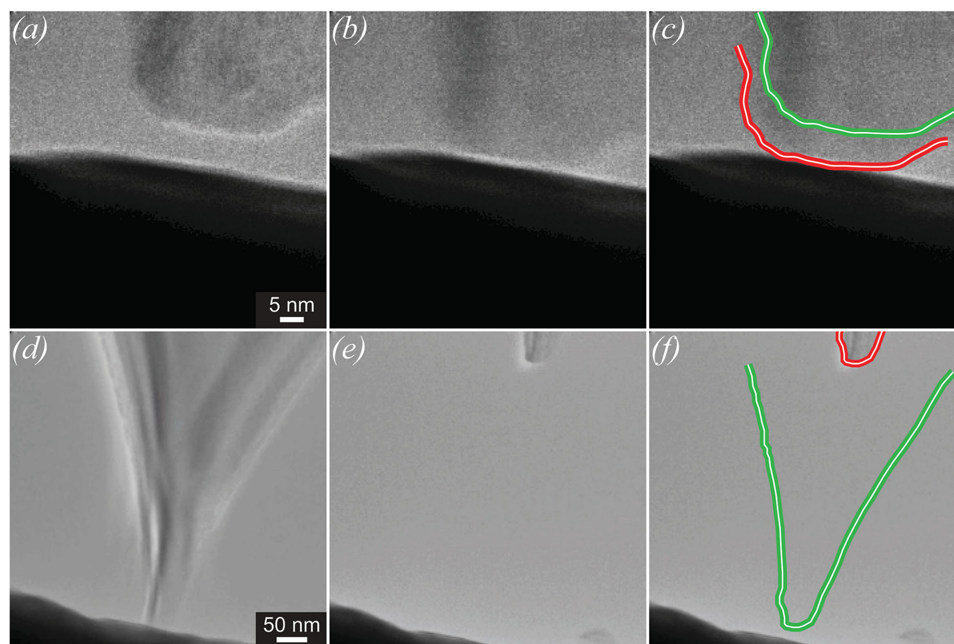

Figure 4. Still images are captured from the video for analysis. Here, the tip is shown a) immediately before snap-in and b) immediately after. c) Red- and green-colored traces of the two positions indicate the relative motion. Likewise, video frames are shown d) before and e) after pull-off, with the difference indicated in (f). From this distance, the pull-off force can be calculated. Note that (e–f) are shown approximately 2 s after the pull-off event, to allow the tip to stabilize for a clear image. Images (a–c) and (d–f), respectively, are at a common magnification.

snap-in distance $d_{\text{snap-in}}$ and the pull-off force $F_{\text{pull-off}}$. From these and the measured tip geometry, $W_{\text{adh,int}}$ and z_0 were extracted using the SNAP method.

Three different nanoscale tips were used in adhesion tests inside the TEM; the probes are shown in their pre-test configurations in Figure 3. For every tip, adhesion tests were performed in at least two distinct locations on the diamond punch to average out effects of local topography and/or variations in the surface chemistry of the punch. For each location, the tips were imaged before the adhesion tests, and then two adhesion tests were performed. Every pull-off test was captured with real-time video such that the magnitude of the snap-in and pull-off events could be measured during post-processing, as described in the Methods section. Extracted values from the adhesion tests at each location are shown in **Figure 5**. Taken together, the averaged values for silicon (with a native oxide) interacting with diamond are $W_{\text{adh,int}} = 0.66 \pm 0.14$ J m^{-2} and $z_0 = 0.25 \pm 0.06$ nm.

The scatter that exists in the data can be attributed to the intrinsic variability of adhesion that occurs even on a perfect diamond (111) single-crystal surface depending on the alignment of the tip and sample atoms. For example, Piotrowski et al.[33] found in atomistic simulations that changing the relative position of two defect-free H-terminated diamond (111) surfaces could lead to 60%–70% changes in the apparent work of adhesion. The scatter may also be due to heterogeneity in the nanoscale topography or composition of the diamond counter surface. To investigate these possibilities further, the surface of the punch was characterized ex situ using AFM and is smooth relative to the sharp tips (RMS roughness of 0.091 nm over a 100 × 100 nm^2 area, as shown in the Supporting Information). However, the flat-punch substrate was not electron transparent and therefore local variations could not be resolved in the TEM. Although the diamond punch was cleaned, with the final step involving exposure to a H plasma, it is possible that the degree of hydrogentation may vary locally. Even with this variability, the measurements are a fundamental improvement over those acquired using conventional techniques (such as the application of spherical contact mechanics), where the roughness is neither measured nor accounted for on either side of the contact. By contrast, knowledge of the Ångstrom-scale tip topography in the present technique enables measurements that can be more meaningfully compared with atomistic models such as those in ref. [33]. Furthermore, and very importantly, despite the scatter the results are meaningfully different from many previously published values as discussed in the following section. While future experiments can incorporate electron transparency of the substrate to account more directly for sample roughness, the present measurements represent a significant advance towards fundamental, predictive adhesion parameters.

3. Discussion

The present experimental results are compared to previously published values for range of adhesion and for work of adhesion. Then, the present measurements are used to calculate values for underlying atomic-scale interactions: the Hamaker constant and the parameters for an interatomic Lennard–Jones interaction. The Hamaker constant and interatomic Lennard–Jones interactions have more direct physical interpretation than

 © 2015 WILEY-VCH Verlag GmbH & Co. KGaA, Weinheim

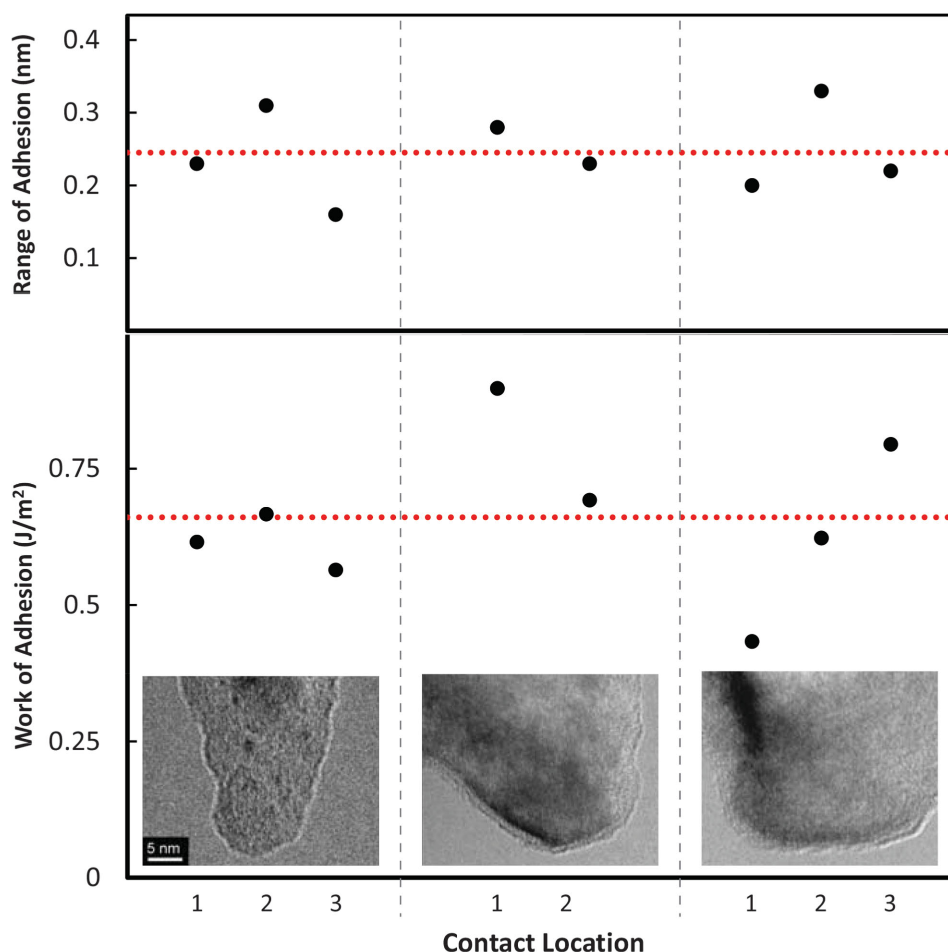

Figure 5. Using the present technique, values of work of adhesion and range of adhesion are extracted simultaneously from in situ adhesion tests. The extracted values of work of adhesion (bottom) and range of adhesion (top) are shown from three different tips, tested in eight distinct locations. Each data point represents the average of two measurements in the same location.

$W_{adh,int}$ and z_0, and can be compared to physics-based theories of van der Waals attraction and also to molecular dynamics simulations.

3.1. Comparing Range of Adhesion to Previously Proposed Values

A survey of the literature shows a wide range of published values of range of adhesion, as listed in **Table 1**. These publications fall into three categories: theoretical studies where the range of adhesion is assumed, often without explanation; experimental studies where the range of adhesion is assumed and that value is used to analyze data; and experimental studies where an indirect measurement of range of adhesion is made. Note that while some of these investigations involve materials or environments different from the present one, many authors[4,48–50,27] claim that z_0 should be approximately equal to the interatomic spacing of typical or specific solids, so useful comparisons can still be made. Therefore, we have normalized the suggested values by the average of the interatomic spacings of the two materials in contact. This should facilitate comparison across material systems.

In the first and second categories, computational or purely theoretical models of contact mechanics are proposed or used, and thus an input value is needed for range of adhesion. As shown in Table 1, the majority of these studies[4,27,31,34,44,45,48–50] estimate the range of adhesion as equal to the interatomic spacing of atoms in the contacting material. While it seems a reasonable ballpark estimate, there is little direct justification provided for this claim. Indeed, with the exception of unreconstructed perfectly commensurate contacting surfaces of identical component materials, it is reasonable to expect that the equilibrium separation should be larger than the interatomic spacing due to lattice defects, topography, and other non-equilibrium features occurring at the surface. To reflect this, some authors estimate larger values ranging from 0.3 to 1 nm.[7,43,46,47] However, data to justify these larger numbers are also lacking. Further, the above authors' assertions about z_0 do not take account of the surrounding environment (vacuum, gas, etc.) through which the interactions occur.

© 2015 WILEY-VCH Verlag GmbH & Co. KGaA, Weinheim

FULL PAPER

Table 1. Values of z_0 that have been proposed in previously published investigations.

Proposed z_0 [nm]	z_0/atom spacing[a)]	Estimated or fit to data	Materials	Refs.
0.16[b)]	1	Estimated	N/A—generic calculation	[4]
0.16[b)]	1	Estimated	N/A—generic calculation	[27]
0.16[b)]	1	Estimated	N/A—generic calculation	[48]
0.16[b)]	1	Estimated	N/A—generic calculation	[49]
0.16[b)]	1	Estimated	N/A—generic calculation	[50]
0.30	N/A	Estimated	N/A—generic calculation	[43]
1.0	N/A	Estimated	N/A—generic calculation	[7]
0.15	0.70	Estimated, used to fit data	Tungsten carbide/diamond	[31]
0.165	0.70	Estimated, used to fit data	Silicon/silicon	[34]
0.20	0.91	Estimated, used to fit data	Platinum/mica	[44]
0.20	0.93	Estimated, used to fit data	Tungsten carbide/diamond	[45]
0.30	1.37	Estimated, used to fit data	Glass/platinum	[46]
0.30	1.40	Estimated, used to fit data	Silicon/ TiO_2	[47]
4–5	28–34	Indirectly calculated	DLC/DLC	[8]

[a)]To enable comparison between different material systems, we normalize by the interatomic spacing. Where two distinct materials are involved, the bond lengths were averaged between them; [b)]These investigations suggest z_0 equal to interatomic spacing; for silicon oxide on diamond, the average of their interatomic spacings is 0.16 nm.

The experimentally determined values in the present study do not support the common assumption that z_0 should be equal to atomic spacing. The interatomic spacings of the component materials are 0.154 nm for single-crystal diamond, 0.234 nm in silicon, and approximately 0.163 nm (the Si—O bond length) for silicon oxide. The measured value of $z_0 = 0.25 \pm 0.06$ nm is larger than all of these values and larger than the average interatomic spacing of the surface materials (0.16 nm is the average of bond length in the diamond and the silicon oxide, 0.18 nm is the arithmetic mean of all three materials).

Only one study[8] was found that falls into the third category, in which an indirect measurement was made of the range of adhesion. Here, the authors perform wear studies on an AFM probe, with periodic measurements of the adhesive force and the probe shape. The probes are initially approximated as paraboloidal, and thus a work of adhesion can be calculated directly from the adhesive force without knowledge of range of adhesion.[4] As the probes wear, they are fit with power-law geometries–for which the adhesive force depends on both work of adhesion and range of adhesion. Here, the work of adhesion is assumed to maintain its pre-wear value throughout the wear test, and then the range of adhesion can be directly calculated. The authors use this method to calculate a range of adhesion of 4–5 nm. In these experiments, the work of adhesion may be changing over the course of a wear test due to changes in surface topography or surface chemistry, so the assumption that it is constant may not be perfectly valid. Further, Grierson et al. attribute the large adhesion range value to either longer-range forces such as capillary action (the investigation was conducted in air) or to surface roughness that is not accounted for in the power law fitting. Also, differences in the properties of the contact materials (density, polarizability, surface topography, and surface contamination) will also have an effect on van der Waals adhesion.

3.2. Comparing Work of Adhesion to Previously Proposed Values

Values of work of adhesion have been far more widely reported than values of z_0; therefore there is a larger body of literature for comparison. While few investigations have directly measured the work of adhesion between a silicon tip and a diamond surface, there have been many prior reports of work of adhesion of related contact pairs: a diamond tip on silicon; a silicon tip in contact with ultrananocrystalline diamond (UNCD) or hydrogenated amorphous carbon (a-C:H) (a form of diamond-like carbon); or any of those materials in a self-mated configuration. While single-crystal diamond contains exclusively sp^3-hybridized carbon in a diamond-cubic packing structure, with some recrystallization and H- or OH-termination on the surface; UNCD is composed of 5–10 nm single-crystal grains, separated by grain boundaries of approximately 0.5 nm thickness, which are composed of a mix of sp^2 and sp^3 carbon.[51] There will be a similar reconstruction and passivation on the surface. Therefore these materials are expected to have similar adhesive interactions, with the biggest difference being surface roughness, which is not often accounted for. Hydrogenated amorphous carbon contains a higher fraction of sp^2 carbon and therefore will behave differently from single-crystal diamond. With regard to dispersion forces specifically,[52] a-C:H has a lower number density of atoms as compared to single-crystal diamond, but the electrical conductivity is much higher, as is the polarizability of atoms. The surface termination and amount of hydrogen on the surface have also been shown to have an effect on work of adhesion.[33]

Relevant measured results for work of adhesion are shown for experimental investigations in **Table 2** and for simulated investigations in **Table 3**. Measured values range widely from 0.01 J m^{-2} (a hydrogen-terminated, self-mated UNCD pair) to 0.83 J m^{-2} (a self-mated silicon contact pair). While the present result ($W_{adh,int}$ = 0.66 J m^{-2}) lies in that range, it is significantly larger than most reported values from similar materials. This difference is attributed to two factors. First, most (but not all) of the AFM studies were performed in air, where contamination and water adsorption can passivate the surface. Second, none of the previous studies took account of surface roughness, which can cause up to an order of magnitude drop in adhesion (as discussed in ref. [42]). When the data from the present study is analyzed under the assumption of parabolic tips (ignoring surface roughness) and using a single-asperity contact model (in accordance with most of the studies in Table 2), the measured work of adhesion is just 0.38 J m^{-2}. This highlights the importance of taking surface roughness into account when quantitative and predictive values of work of adhesion are needed.

The measurements presented here are acquired in the TEM, where the background pressure is approximately 10^{-6} Pa. Many adhesion measurements are conducted in ambient conditions.

© 2015 WILEY-VCH Verlag GmbH & Co. KGaA, Weinheim

Table 2. Values of W_{adh} that have been measured in previously published experimental investigations of relevant contact pairs.

Tip/substrate materials	Measured W_{adh} [J m^{-2}]	Comment	Refs.
Diamond/silicon (111)	0.20–0.45[a)]	Interfacial force microscope	[35]
Silicon/DLC	0.08	AFM, air; tip characterized	[8]
DLC/DLC	0.05		
Silicon/ta-C	0.10–0.35	AFM, air; tip characterized	[40]
Diamond/UNCD	0.06	AFM, in air	[12]
Diamond/UNCD-H[b)]	0.01	AFM, in air	
Silicon/silicon	0.83	AFM, in air	
Silicon/silicon	0.13–0.35	AFM, in air	[34]
Silicon/silicon	0.12	AFM, in air	[32]
Amorphous C/diamond (111)-H	0.10	AFM, UHV[c)], R_{tip} = 45 nm	[33]
Amorphous C/diamond (111)-H	0.03	AFM, UHV, R_{tip} = 150 nm	
Amorphous C/diamond (111)-H	0.19	AFM, UHV, R_{tip} = 45 nm	
Amorphous C /diamond (111)-H	0.05	AFM, UHV, R_{tip} = 150 nm	

[a)]Radius not well characterized; quoted as "<10 nm." Also value decreased with time elapsed; [b)]An appended "-H" indicates that the surface was intentionally hydrogen terminated; [c)]"UHV" designates an environment of ultra-high vacuum.

This will result in different surface chemistries than what is found in vacuum, and can lead to the formation of a water meniscus condensed at the tip-sample contact. If that occurs, the meniscus will make a contribution to adhesion in addition to the solid–solid interaction discussed here.[53] It is likely that the nature of the meniscus contribution will be affected by the tip roughness, potentially quite strongly, since the geometry of the contact is crucial in determining the properties of the meniscus.[54] We note that a meniscus is not automatically present when one works in ambient conditions. It has been shown that in some cases (e.g., with low-to-moderate relative humidities, with hydrophobic materials, or at high sliding speeds) meniscus nucleation may not occur, and so solid–solid adhesion will determine the adhesive behavior.[55,56] Thus, the solid–solid parameters that can be determined from the method presented here may be relevant for a number of contacts in ambient conditions. Furthermore, the present approach—high-resolution tip imaging, and recording of the snap-in distance and pull-off force—could be further developed to help quantify how a meniscus contributes to adhesion.

3.3. Calculating the Resultant Hamaker Constant from the Measured Quantities

To connect the measured parameters to physical quantities, we first use the work of adhesion $W_{adh,int}$ to calculate the Hamaker constant under the assumption that the adhesion is purely due to van der Waals interactions. The Hamaker constant $A_{1:2}$ describes the strength of interaction between materials (designated 1 and 2) interacting across a vacuum and is a function of the density and polarizability of the interacting materials. The work of adhesion and Hamaker constant between two planar surfaces experiencing van der Waals attraction can be related by ignoring repulsion and using the following equation:[57]

$$W_{adh} = \frac{A_{1:2}}{12\pi D_0^2}, \quad (2)$$

where D_0 represents an artificial cut-off distance for minimum separation. Unfortunately, the correct choice for D_0 in this calculation is not entirely clear, as discussed further in the Supporting Information. Israelachvili[57] suggests the use of the interatomic distance divided by

Table 3. Values of W_{adh} that have been measured in previously published simulation investigations of relevant contact pairs.

Tip/substrate materials	Measured W_{adh} [J m^{-2}]	Comment	Refs.
Diamond (111) flat[a)]/diamond (111)	0.20–0.30	Depends on H coverage	[33]
High-sp^3 carbon flat/diamond (111)	0.15–0.23		
Low-sp^3 carbon flat/diamond (111)	0.15–0.25		
MDN[b)] flat/diamond (111)	0.03–0.15	Depends on roughness	
Diamond (001) flat/diamond (001)	0.15–0.25	Depends on H coverage	
Low-sp^3 carbon flat/diamond (001)	0.10		
UNCD tip[c)]/diamond (111)	0.60	Simulated AFM-like tests	[52]
UNCD tip/diamond (111)-H	0.35		
UNCD tip/UNCD	0.40		
UNCD tip/UNCD-H	0.20		
UNCD tip/DLC-H	0.10		
UNCD-H tip/diamond (111)	0.24		
UNCD-H tip/diamond (111)-H	0.28		
UNCD-H tip/UNCD	0.26		
UNCD-H tip/UNCD-H	0.18		
UNCD-H tip/DLC-H	0.10		
DLC-H tip/diamond (111)	0.12		
DLC-H tip/diamond (111)-H	0.12		
DLC-H tip/UNCD	0.12		
DLC-H tip/UNCD-H	0.10		
DLC-H tip/DLC-H	0.08		

[a)]Unlike AFM, contact involved nominally planar surfaces. W_{adh} is calculated by integrating the force during separation and should be considered a $W_{adh,eff}$; [b)]MDN stands for "model diamond nanocomposite;" [c)]Similar to AFM, contact involved a 2.5-nm tip on a flat surface. W_{adh} calculated using continuum contact model (DMT), using a best-fit paraboloid tip.

© 2015 WILEY-VCH Verlag GmbH & Co. KGaA, Weinheim

2.5 as an empirical rule that applies to a wide variety of compounds. Therefore, using the arithmetic mean of the interatomic spacings of diamond and silicon oxide (0.154 and 0.163 nm, respectively) and dividing by 2.5 yields $D_0 = 0.063$ nm. This in turn yields a Hamaker constant $A_{\mathrm{Si:C}} = 9.9 \times 10^{-20}$ J. For comparison, theoretical calculations of the Hamaker constants for the component materials ($A_{\mathrm{C:C}}$ and $A_{\mathrm{SiO2:SiO2}}$ of 3.0×10^{-19} and 6.5×10^{-20} J, respectively)[57] can be combined to describe contact between dissimilar surfaces using the semi-empirical combining rule $A_{1:2} = \sqrt{A_{1:1}A_{2:2}}$ (the geometric mean). This yields an expected Hamaker constant of $A_{\mathrm{C:Si}} = 1.4 \times 10^{-19}$ J. This is 40% larger than the experimentally derived value; the difference can be attributed to the fact that the expected value ignored surface effects such as reconstruction and passivation of bonds.[33] This further demonstrates the importance of measuring an experimental value for a given environment and set of conditions, rather than relying on reference values.

3.4. Calculating the Interatomic Lennard–Jones Parameters from the Measured Quantities

The interatomic Lennard–Jones 6–12 potential is an approximate mathematical description of the energy of interactions between two atoms, and has two independent parameters, σ_{LJ} and $\varepsilon_{\mathrm{LJ}}$.[57] It has been more extensively studied and verified (for instance, by its use in the AIREBO potential of molecular dynamics simulation)[58] than the Lennard–Jones surface potential (discussed in Section 5). By integrating the interatomic potential over two infinite half-spaces and then comparing terms, the interatomic parameters can be calculated as follows:[59]

$$\sigma_{LJ} = \left(\frac{15}{2}\right)^{1/6} z_0 \tag{3}$$

$$\varepsilon_{LJ} = \frac{A}{4\pi^2 \rho_1 \rho_2 \sigma^6} \tag{4}$$

where ρ_1, ρ_2 designate the number density of atoms in the two interacting solids. Assuming values for number density of atoms in diamond and thermal silicon oxide (1.76×10^{29} and 2.28×10^{28} m^{-3}, respectively)[60] and using the Hamaker constant calculated above ($A_{\mathrm{Si:C}} = 9.9 \times 10^{-20}$ J), fitting to the experimental results yields $\sigma_{LJ} = 0.35$ nm and $\varepsilon_{LJ} = 3.4 \times 10^{-22}$ J = 0.0021 eV. For comparison, empirical values from the molecular dynamics literature are 0.34 nm and 0.00284 eV for carbon[58] and 0.22 nm and 0.0021 eV for silicon.[61] As with the Hamaker constant, the geometric mean of these two values is appropriate for ε_{LJ}, while an arithmetic mean is used to combine σ_{LJ};[58] yielding combined empirically derived values of $\sigma_{LJ,\mathrm{Si:C}} = 0.28$ nm and $\varepsilon_{LJ,\mathrm{Si:C}} = 0.0024$ eV. These empirically derived values are in reasonable agreement with the values measured here. Differences between them are not surprising because: a) these empirically derived values are for single-crystal materials (ignoring surface contamination, oxidation, and reconstruction); and b) empirical combining rules were used.

4. Conclusion

In this paper, a novel technique was used for simultaneously extracting fundamental, geometry-independent interaction parameters—intrinsic work of adhesion and range of adhesion—for two effectively rigid materials described using a two-parameter adhesion law. Fully in situ adhesion tests were performed with silicon AFM probes containing a native oxide contacting a diamond substrate in vacuum. The measured value of intrinsic work of adhesion, $W_{\mathrm{adh,int}} = 0.66 \pm 14$ J m^{-2}, was significantly higher than most previous experimental and simulation measurements. The difference may be due to the fact that we explicitly account for surface roughness down to the sub-nanometer scale, unlike previous measurements. Importantly, this value is 70% higher than the value that would have been measured under assumptions that are common in AFM testing (parabolic tip, DMT model). This demonstrates the critical importance of accounting for Ångström-scale roughness in nanocontacts. The measured range of adhesion, $z_0 = 0.25 \pm 0.06$ nm, represents the most direct experimental measurement of this quantity to date. It falls within the range of previous measurements, but is larger than the value predicted using the common estimation that the range of adhesion is equal to the atomic spacing of the component materials. Finally, the measured quantities were used to estimate values of the Hamaker constant (assuming pure van der Waals interactions) and of the parameters needed to represent the adhesion between these materials using a Lennard–Jones interatomic potential; physically reasonable values are obtained. More broadly, we have demonstrated a novel and general technique for experimentally determining two independent interaction parameters—the length scale and the strength of the adhesion—that can comprehensively describe the adhesive interaction between a pair of materials. Knowledge of these parameters enables the use of continuum models for prediction of adhesion forces and contact behavior in any arbitrary contact geometry.

5. Experimental Section

Summarizing the Novel Snap-in/Pull-off Numerical Adhesion Parameter Method: The SNAP method is a numerical technique for simultaneously determining the work of adhesion and range of adhesion from knowledge of three measurements from an AFM-like adhesion test: 1) the tip shape; 2) the adhesive force; and 3) the position during approach at which the snap-in instability[62] occurs. The SNAP method is summarized here, and described in more detail in ref. [20]. Mathematically, the total interaction force between the tip and sample $F_{\mathrm{tip/sample}}$ can be calculated by integrating the commonly used Lennard–Jones 3–9 traction-separation relation[4,5,8,48] over the geometry of the tip. More specifically, the normal stress σ_{normal} acting between the tip and sample for any differential element of tip area can be computed (as a function of separation distance z_{sep}) by using the Lennard–Jones 3–9 traction–separation relation:[5]

$$\sigma_{\mathrm{normal}}\left(z_{\mathrm{sep}}\right) = -\frac{8W_{\mathrm{adh,int}}}{3z_0}\left[\left(\frac{z_0}{z_{\mathrm{sep}}}\right)^3 - \left(\frac{z_0}{z_{\mathrm{sep}}}\right)^9\right] \tag{5}$$

Then, integration of this equation over the full tip geometry yields the tip/sample interaction force $F_{\mathrm{tip/sample}}$ as a function of tip/sample separation distance d:

© 2015 WILEY-VCH Verlag GmbH & Co. KGaA, Weinheim

$$F_{\text{tip/sample}} = \int_{Area} \sigma_{\text{normal}}(z_{\text{sep}})\,dA = \int_0^{2\pi}\int_0^{\infty} \sigma_{\text{normal}}(z_{\text{sep}}(r,\theta))\,r\,dr\,d\theta = \int_0^{\infty}\left\{\frac{8W_{\text{adh,int}}}{3z_0}\left[\left(\frac{z_0}{z_{\text{tip}}+d}\right)^3 - \left(\frac{z_0}{z_{\text{tip}}+d}\right)^9\right]\right\}2\pi r\,dr \quad (6)$$

Note that the separation of any differential element of area is the sum of its height on the tip z_{tip} and the tip/sample separation distance (i.e., $z_{sep}= z_{tip}+ d$). Once the $F_{tip/sample}(d)$ is known, then the computed adhesive force and snap-in distance can be calculated for a wide range of input values of $W_{adh,int}$ and z_0. By matching the computed values of adhesive force and snap-in distance to the measured values, the correct $W_{adh,int}$ and z_0 can be extracted. In general, with tips of arbitrary geometry, only a single pair of ($W_{adh,int}$, z_0) values will correctly predict the measured values.

Apparatus and Materials for Fully In Situ Adhesion Testing: In the present experiments, a TEM nanoindenter (Picoindenter PI-95, Hysitron Inc., Minneapolis, MN) is used to perform in situ adhesion testing inside of a TEM (2010F, JEOL, Tokyo, Japan). The TEM has a field-emission source and was operated at a 200-keV accelerating voltage. Each adhesion test was conducted by bringing the flat punch indenter tip into contact with a calibrated[63] AFM cantilever, which is mounted rigidly on the sample stage of the nanoindenter, as shown in Figure 2. The flat punch indenter tip mimics the flat substrate that is inserted into a traditional AFM and, as with such an instrument, the force exerted by the sample on the tip is monitored by detecting the deflection of the cantilever—in this case using direct imaging of the vertical deflection of the cantilever's tip.

Three AFM probes (PPP-CONT, Nanosensors, Neuchatel, Switzerland) were tested against a flat indenter tip (Flat Punch probe, Hysitron, Minneapolis, MN). The probes are composed of silicon with a native oxide and contain a sharp nanoscale tip; no special preparation was performed except to mount the probes on the indenter stage. The spring constants of the three cantilevers were 0.239, 0.199, and 0.162 N m^{-1} for the tips shown in Figure 3a, b, c, respectively. Contact-mode cantilevers were chosen to maximize the force sensitivity. The flat punch indenter was composed of single-crystal diamond, terminating in a (100) face. The punch was mechanically cleaned with acetone on a cotton swab, followed by 20 min of sonication in each of isopropanol, acetone, and methanol, followed by a 5-min oxygen/hydrogen treatment in a plasma cleaner (Solarus 950, Gatan, Inc., Pleasanton, CA). The RMS roughness of the diamond punch was 0.091 nm as measured using ex situ scanning over several 100×100 nm^2 areas using an AFM (MFP-3D, Asylum Research, Santa Barbara, CA). The topography image is shown in the Supporting Information. The geometries of the sharp silicon probe apexes were determined using high-resolution TEM imaging of the AFM tips when out of contact. These images are used to characterize the profile of the tip in detail before testing, and permit much higher magnification images than are achievable during the adhesion test itself, when the surfaces are moving.

Determination of Tip Shape, Pull-off Force and Snap-in Distance: High-resolution TEM images of the tip were taken immediately before the adhesion tests were performed, similar to those shown in Figure 3. The Ångström-scale morphology of these tips were measured by tracing the outer contours of the tip using post-processing image analysis, using a technique similar to ref. [64], as shown in **Figure 6**. In order to compare with the DMT single-asperity contact models, a circle has been fit to each contour in order to extract the best-fit radius to be used in calculations. Parabolic fits to these contours yielded nearly identical effective radii. The 3D shape of the probes was assumed to be axisymmetric, in accordance with prior studies.[64]

The adhesion tests were then immediately conducted inside the same TEM. The indenter punch was brought toward the AFM probe at a rate of 1 nm s^{-1}. As the punch approached, there was an observable "snap-in" event, in which the AFM cantilever suddenly deflected, bringing the tip in contact with the punch. After contact was established, the direction of motion of the indenter punch was reversed. Upon retraction, adhesion held the tip and punch in contact, causing the cantilever to elastically deflect in the direction of the punch. Eventually, the tip/punch contact separated suddenly in a "pull-off" event, in which the AFM cantilever suddenly returns to its free (unloaded) position.

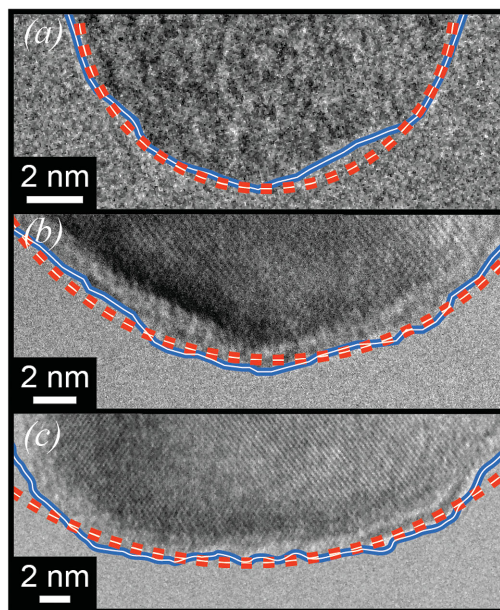

Figure 6. The shape of the tip was measured using high-resolution TEM images. The outer contour (solid, blue line) was traced based on contrast variation, and was used in the calculation of W_{adh} and z_0. For the comparison calculation using the single-asperity DMT model, a circle was fit to the data (red, dashed line) for extraction of a best-fit radius.

The adhesion tests were recorded using a video-rate camera at approximately 30 frames per second, and captured using a digital video recorder. An example video of a typical adhesion test can be found in the Supporting Information. In post-processing, the motion of the AFM tip is measured at all points throughout the test relative to its free, unloaded position. Additionally, the motion of the tip is a direct measurement of the elastic deflection Δ of the cantilever, and can be multiplied by the spring constant of the cantilever, k_{lever}, to calculate the total interaction force ($F_{total} = k_{lever} \cdot \Delta$). The magnitude of the deflection during snap-in $d_{snap\text{-}in}$ was recorded. The magnitude of the deflection during pull-off was also recorded, and multiplied by the spring constant of the lever to determine the value of the pull-off force $F_{pull\text{-}off}$.

A final experimental consideration is the effect of vibration of the nanoindenter. The nanoindenter tip is spring-mounted and exhibits constant vibration at the natural resonance frequency of the force transducer, which for the present apparatus is 119.8 Hz. Therefore, the apparent position of the indenter tip in the video (which is captured at 30 frames per second) is the time-averaged position; the actual position of the spring-mounted indenter varies around this average approximately sinusoidally with time. Immediately prior to every set of experiments, several at-rest displacement measurements were taken to characterize the standard deviation of the vibration at that specific time and day. The vibration is determined by measuring the capacitance of a three-plate capacitor system in which the tip is rigidly attached to the central plate (similar to what is described in ref. [65]). This varied throughout the day and depended on the use of other active nearby equipment and various external variables. The time-scale for snap-in to occur is on the order of a single period of vibration of the AFM cantilever, which for a typical cantilever resonance frequency of 10 kHz is 0.1 ms. This is approximately two orders of magnitude faster than the period of oscillation for the nanoindenter tip. Therefore, the indenter's displacement noise can be considered as quasistatic, and thus the true snap-in distance relevant for adhesion characterization is the distance of closest approach during the nanoindenter's oscillation, not the

© 2015 WILEY-VCH Verlag GmbH & Co. KGaA, Weinheim

time-averaged position of the nanoindenter tip. Thus, the true value for snap-in $d_{\text{snap-in,true}}$ is smaller than the measured (time-averaged) distance $d_{\text{snap-in,meas.}}$ by the amplitude of the nanoindenter's vibration A_{vib} and, for sinusoidal vibration, is given by:

$$d_{\text{snap-in,true}} = d_{\text{snap-in,meas}} - A_{\text{vib}} = d_{\text{snap-in,meas}} - \sqrt{2}\sigma_{\text{vib}}, \quad (7)$$

where σ_{vib} is the standard deviation of vibration that is measured before experimentally. The value of σ_{vib} was 1.34 nm for the test shown in Figure 4, and 2.67 and 1.21 nm for the tips shown in Figure 3a,b, respectively. Thus, the snap-in distance used to extract adhesion parameters is the true value of snap-in, calculated according to Equation (7).

Supporting Information

Supporting Information is available from the Wiley Online Library or from the author.

Acknowledgements

The authors acknowledge useful discussions with K. Turner and D. Grierson, as well as atomic force microscopy assistance by G. Wabiszewski. Use of the Nanocharacterization Facility at the University of Pennsylvania is acknowledged. R.W.C and T.D.B.J. acknowledge support from National Science Foundation under award No. CMMI12–00093. R.W.C., T.D.B.J., and J.A.L. acknowledge support from the UPenn MRSEC Program of the National Science Foundation under award No. DMR11–20901. R.W.C acknowledges support from AFOSR under Contract No. FA2386–14–1–4071 AOARD.

Received: December 11, 2014
Revised: March 8, 2015
Published online: May 13, 2015

[1] C. M. Mate, *Tribology on the Small Scale: a Bottom Up Approach to Friction, Lubrication, and Wear*, Oxford University Press, Oxford, UK **2008**.
[2] D. Maugis, *Contact, Adhesion and Rupture of Elastic Solids*, Springer, Berlin, Heidelberg, **2000**.
[3] C.-Y. Hui, R. Long, *J. Adhes.* **2012**, *88*, 70.
[4] D. Maugis, *J. Coll. Int. Sci.* **1992**, *150*, 243.
[5] J. A. Greenwood, *Phil. Mag.* **2009**, *89*, 945.
[6] Z. Zheng, J. Yu, *J. Coll. Int. Sci.* **2007**, *310*, 27.
[7] H. Yao, M. Ciavarella, H. Gao, *J. Coll. Int. Sci.* **2007**, *315*, 786.
[8] D. S. Grierson, J. Liu, R. W. Carpick, K. T. Turner, *J. Mech. Phys. Sol.* **2013**, *61*, 597.
[9] B. Persson, *Phys. Rev. Lett.* **2002**, *89*, 245502.
[10] C. H. Mastrangelo, C. H. Hsu, *Solid-State Sensor and Actuator Workshop, 5th Technical Digest, IEEE* **1992**, 208.
[11] J. Q. Feng, *J. Coll. Int. Sci.* **2001**, *238*, 318.
[12] A. Sumant, D. Grierson, J. Gerbi, J. Carlisle, O. Auciello, R. Carpick, *Phys. Rev. B* **2007**, *76*, 235429.
[13] B. Cappella, G. Dietler, *Surf. Sci. Rep.* **1999**, *34*, 1.
[14] F. J. Giessibl, *Rev. Mod. Phys.* **2003**, *75*, 949.
[15] R. Garcia, R. Perez, *Surf. Sci. Rep.* **2002**, *47*, 197.
[16] S. P. Jarvis, A. Oral, T. P. Weihs, J. B. Pethica, *Rev. Sci. Instrum.* **1993**, *64*, 3515.
[17] S. P. Jarvis, H. Yamada, S.-I. Yamamoto, H. Tokumoto, *Rev. Sci. Instrum.* **1996**, *67*, 2281.
[18] P. D. Ashby, L. W. Chen, C. M. Lieber, *J. Am. Chem. Soc.* **2000**, *122*, 9467.
[19] S. A. Joyce, J. E. Houston, *Rev. Sci. Instrum.* **1991**, *62*, 710.
[20] T. D. B. Jacobs, J. A. Lefever, R. W. Carpick, *Tribol. Lett.* **2015,** DOI: 10.1007/s11249-015-0539-9.
[21] O. Auciello, S. Pacheco, A. Sumant, C. Gudeman, S. Sampath, A. Datta, R. Carpick, V. Adiga, P. Zurcher, Z. Ma, H.-C. Yuan, J. Carlisle, B. Kabius, J. Hiller, S. Srinivasan, *IEEE Microwave* **2007**, *8*, 61.
[22] F. W. DelRio, M. P. de Boer, J. A. Knapp, E. David Reedy, P. J. Clews, M. L. Dunn, *Nat. Mater.* **2005**, *4*, 629.
[23] K. T. Turner, S. M. Spearing, *Proc. Roy. Soc. A* **2005**, *462*, 171.
[24] R. Maboudian, C. Carraro, *Annu. Rev. Phys. Chem.* **2004**, *55*, 35.
[25] N. Miki, S. M. Spearing, *J. Appl. Phys.* **2003**, *94*, 6800.
[26] B. N. J. Persson, E. Tosatti, *J. Chem. Phys.* **2001**, *115*, 5597.
[27] B. V. Derjaguin, V. M. Muller, Y. P. Toporov, *J. Colloid Interface* **1975**, *53*, 314.
[28] K. L. Johnson, K. Kendall, A. D. Roberts, *Proc. Roy. Soc. A* **1971**, *324*, 301.
[29] K. Fuller, D. Tabor, *Proc. Roy. Soc. A* **1975**, *345*, 327.
[30] D. Maugis, *J. Adhes. Sci. Technol.* **1996**, *10*, 161.
[31] D. Grierson, E. Flater, R. Carpick, *J. Adhes. Sci. Technol.* **2005**, *19*, 291.
[32] A. V. Sumant, D. S. Grierson, J. E. Gerbi, J. Birrell, U. D. Lanke, O. Auciello, J. A. Carlisle, R. W. Carpick, *Adv. Mater.* **2005**, *17*, 1039.
[33] P. L. Piotrowski, R. J. Cannara, G. Gao, J. J. Urban, R. W. Carpick, J. A. Harrison, *J. Adhes. Sci. Technol.* **2010**, *24*, 2471.
[34] D. L. Liu, J. Martin, N. A. Burnham, *Appl. Phys. Lett.* **2007**, *91*, 043107.
[35] N. W. Moore, J. E. Houston, *J. Adhes. Sci. Technol.* **2010**, *24*, 2531.
[36] R. G. Horn, J. N. Israelachvili, F. Pribac, *J. Coll. Int. Sci.* **1987**, *115*, 480.
[37] H. K. Christenson, *J. Phys. Chem.* **1993**, *97*, 12034.
[38] K. Chung, Y. Lee, D. Kim, *Ultramicroscopy* **2005**, *102*, 161.
[39] K.-H. Chung, D.-E. Kim, *Ultramicroscopy* **2007**, *108*, 1.
[40] J. Liu, J. K. Notbohm, R. W. Carpick, K. T. Turner, **2010**, *ACS Nano*, *4*, 3763.
[41] J. Liu, D. Grierson, N. Moldovan, J. Notbohm, S. Li, P. Jaroenapibal, S. O'Connor, A. Sumant, N. Neelakantan, J. Carlisle, *Small* **2010**, *6*, 1140.
[42] T. D. B. Jacobs, K. E. Ryan, P. L. Keating, D. S. Grierson, J. A. Lefever, K. T. Turner, J. A. Harrison, R. W. Carpick, *Tribol. Lett.* **2013**, *50*, 81.
[43] B. Persson, *Wear* **2003**, *254*, 832.
[44] R. W. Carpick, N. Agrait, D. F. Ogletree, M. Salmeron, *J. Vac. Sci. Tech. B* **1996**, *14*, 1289.
[45] M. Enachescu, R. van den Oetelaar, R. W. Carpick, D. F. Ogletree, C. Flipse, M. Salmeron, *Phys. Rev. Lett.* **1998**, *81*, 1877.
[46] Y. Rabinovich, *J. Coll. Int. Sci.* **2000**, *232*, 17.
[47] J. Katainen, M. Paajanen, E. Ahtola, V. Pore, J. Lahtinen, *J. Coll. Int. Sci.* **2006**, *304*, 524.
[48] J. Greenwood, *Proc. Roy. Soc. A* **1997**, *453*, 1277.
[49] D. Tabor, *J. Coll. Int. Sci.* **1977**, *58*, 2.
[50] V. M. Muller, V. S. Yushchenko, B. V. Derjaguin, *J. Coll. Int. Sci.* **1980**, *77*, 91.
[51] O. Auciello, J. Birrell, J. A. Carlisle, J. E. Gerbi, X. Xiao, B. Peng, H. D. Espinosa, *J. Phys. Condens. Matter* **2004**, *16*, R539.
[52] K. E. Ryan, P. L. Keating, T. D. Jacobs, D. S. Grierson, K. T. Turner, R. W. Carpick, J. A. Harrison, *Langmuir* **2014**, *30*, 2028.
[53] D. B. Asay, M. P. de Boer, S. H. Kim, *J. Adhes. Sci. Technol.* **2010**, *24*, 2363.
[54] M. P. de Boer, P. C. T. de Boer, *J. Coll. Int. Sci.* **2007**, *311*, 171.
[55] C. Greiner, J. R. Felts, Z. Dai, W. P. King, R. W. Carpick, *ACS Nano* **2012**, *6*, 4305.
[56] E. Riedo, F. Lévy, H. Brune, *Phys. Rev. Lett.* **2002**, *88*, 185505.
[57] J. N. Israelachvili, *Intermolecular and Surface Forces*, Academic Press, San Francisco, CA **2011**.

© 2015 WILEY-VCH Verlag GmbH & Co. KGaA, Weinheim

[58] S. Stuart, A. Tutein, J. A. Harrison, *J. Chem. Phys.* **2000**, *112*, 6472.
[59] N. Yu, A. A. Polycarpou, *J. Coll. Int. Sci.* **2004**, *278*, 428.
[60] D. R. Lide, *CRC Handbook of Chemistry and Physics*, CRC Press, London, England, **2004**.
[61] P. M. Zimmerman, M. Head-Gordon, A. T. Bell, *J. Chem. Theory Comput.* **2011**, *7*, 1695.
[62] H.-J. Butt, B. Cappella, M. Kappl, *Surf. Sci. Rep.* **2005**, *59*, 1.
[63] J. E. Sader, J. A. Sanelli, B. D. Adamson, J. P. Monty, X. Wei, S. A. Crawford, J. R. Friend, I. Marusic, P. Mulvaney, E. J. Bieske, *Rev. Sci. Instrum.* **2012**, *83*, 103705.
[64] T. D. B. Jacobs, R. W. Carpick, *Nat. Nanotechnol.* **2013**, *8*, 108.
[65] B. Bhushan, A. V. Kulkarni, W. Bonin, J. T. Wyrobek, *Phil. Mag. A* **1996**, *74*, 1117.

© 2015 WILEY-VCH Verlag GmbH & Co. KGaA, Weinheim